JOURNAL OF MATERIALS SCIENCE 35 (2000) 2155–2165

Synthesis, microstructure and properties characterization of disintegrated melt deposited Mg/SiC composites

M. GUPTA, M.O. LAI, D. SARAVANARANGANATHAN
Department of Mechanical and Production Engineering, National University of Singapore, 10 Kent Ridge Crescent, Singapore 119260
E-mail: mpegm@nus.edu.sg

In the present study, elemental and silicon carbide reinforced magnesium materials were synthesized using an innovative disintegrated melt deposition method followed by hot extrusion. Microstructural characterization studies revealed the presence of minimal porosity and completely recrystallized matrix in all the unreinforced and reinforced samples. In the case of reinforced magnesium samples, a fairly uniform distribution of SiC particulates and good SiC-Mg interfacial integrity was realized. The results of microhardness measurements revealed an increase in the brittleness of the SiC-Mg interfacial region with an increase in the amount of SiC particulates. Results of physical and mechanical properties characterization revealed that the increasing presence of SiC particulates led to an increase in hardness and elastic modulus, does not affect 0.2% yield strength and reduces the ultimate tensile strength, ductility, work for fracture and coefficient of thermal expansion. An attempt is made to correlate the results of physical and mechanical properties testing with that of the microstructural characterization.

1. Introduction

Magnesium is one of the lightest structural elements known to design engineer. With its ∼35% lower density when compared to aluminum, it carries tremendous potential for engineering applications requiring high specific mechanical properties. One of the major limitations of magnesium and its alloys is their low elastic modulus, which limits its use in conventional and critical engineering applications as structural material. With the advent of metal matrix composites, it has become possible to increase the stiffness and hardness of the metallic matrices by addition of stiffer and harder ceramic particulates. In addition, judicious selection of type, size and volume fraction of ceramic particulates for a given metallic matrix also assists in realizing enhanced tribological characteristics, dimensional stability, damping capacity and elevated temperature creep properties [1, 2].

In recent years, attempts have been made to synthesize ceramic reinforced magnesium based materials using a number of synthesis methodologies that can essentially be categorized into three distinct groups. These include liquid-phase processes (such as conventional casting [3] and squeeze casting [4]), two-phase processes (such as compocasting [5]) and the solid-phase processes (such as powder based methods [2]). The matrix materials commonly investigated in the case of magnesium based composites include commercial alloys such as AZ61, AZ91 and AZ91D while silicon carbide (SiC) remains the most commonly selected reinforcement phase [1–5]. The results of literature search, however, revealed that no study is carried out to synthesize the magnesium-based composites using the spray-type techniques, which involve the disintegration of molten composite stream prior to deposition. In addition, extremely limited information interrelating processing, microstructure and mechanical properties of SiC reinforced elemental magnesium is available for any processing technique reported so far by the investigators [1–5].

Accordingly, the primary aim of the present study was to present to the research community the microstructural, physical and mechanical characteristics of the elemental and SiC reinforced magnesium synthesized using an innovative processing technique commonly known as disintegrated melt deposition [6]. Microstructural, physical and mechanical properties characterization studies were made so as to understand the influence of SiC particulates on the response of pure magnesium matrix in the absence of any other effects that may arise as a result of presence of alloying elements. Particular emphasis was placed to understand the processing-microstructure-properties interrelationship in the case of magnesium containing increasing amount of SiC particulates.

2. Experimental procedures

2.1. Materials

In this study, pure magnesium of 99.5% purity was used as the base material and silicon carbide (α-SiC)

particulates, with an average size of 25 μm, were used as the ceramic reinforcement phase.

2.2. Processing

The synthesis of the elemental magnesium (Mg) and magnesium based composites (Mg/SiC) containing three different amounts of SiC particulates was carried out using disintegrated melt deposition (DMD) technique. For Mg/SiC composites, the synthesis procedure involved superheating the magnesium chips with SiC particulates to 750°C under inert atmosphere in a graphite crucible followed by stirring of the melt in the range of 450–460 rpm for about 5 minutes. The stirring was conducted in order to facilitate the incorporation and uniform distribution of the SiC particulates in the metallic matrix. Following stirring, the composite melt was poured through a 10 mm centrally drilled hole in the graphite crucible and the resultant stream was disintegrated using two linear argon gas jets at a distance of 0.20 m from the melt pouring point. The gas flow rate was maintained at 4.17×10^{-4} m^3/s. The disintegrated composite melt slurry was subsequently deposited on a circular shaped metallic substrate located at 0.242 m from the gas disintegration point. Synthesis of elemental magnesium (Mg) was carried out using the same procedure described above except for the absence of SiC particulates. Both Mg and Mg/SiC materials were synthesized under argon atmosphere so as to minimize oxidation of magnesium. Fig. 1 shows a schematic diagram of the experimental set-up used in the present study.

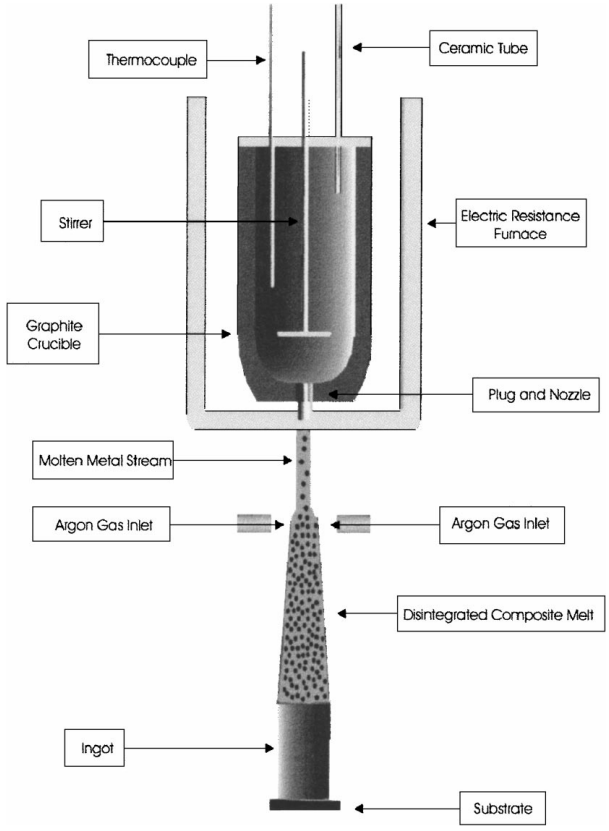

Figure 1 Schematic diagram showing the experimental set-up used in the present study.

2.3. Secondary processing

Mg and Mg/SiC ingots obtained following disintegrated melt deposition were machined to a diameter of 35 mm and hot extruded at 350 °C employing a reduction ratio of 13 : 1 on a 150 ton hydraulic press using colloidal graphite as the lubricant.

2.4. Quantitative assessment of SiC particulates

Quantitative assessment of SiC particulates in the Mg/SiC samples was carried out using the chemical dissolution method. Chemical dissolution method involved: (i) measuring the mass of the composite samples, (ii) dissolving the samples in hydrochloric acid, followed by (iii) filtering to isolate the ceramic particulates. The particulates were then dried and the weight fraction determined [6].

2.5. Density measurements

The densities of the extruded Mg and Mg/SiC samples were measured by Archimedes' principle to quantify the volume fraction of porosity. The density measurements involved weighing polished discs of the extruded samples in air and when immersed in distilled water. The densities, derived from the recorded weights, were then compared to the theoretical Rule of Mixtures densities from which the volume fractions of porosity were calculated. The samples were weighed using an A&D ER-182A electronic balance to an accuracy of ± 0.0001 g [6].

2.6. Microstructural characterization

Microstructural characterization studies were conducted on the extruded Mg and Mg/SiC samples in order to determine the size and shape, and morphological characteristics of grains, distribution of SiC particulates, presence of porosity, and interfacial characteristics of SiC with the magnesium matrix.

Microstructural characterization was carried out on the unetched and etched Mg and Mg/SiC samples using an optical (Olympus BH2-UMA) and JEOL scanning electron microscopes (SEM) equipped with energy dispersive spectroscopy (EDS). Acetic glycol solution was used for both Mg and Mg/SiC samples in the present study to reveal the grain boundaries for microstructural analysis. The average grain sizes and their morphological characteristics were determined using image analysis. Image analysis was performed using 520 Quantimet image analysis system and was also used to characterize the morphological aspects of SiC particulates in the extruded Mg/SiC samples.

2.7. X-Ray diffraction studies

X-ray diffraction study was carried out on Mg and Mg/SiC samples using an automated *Shimadzu* LAB-X XRD-6000 diffractometer. Thin samples (10 mm diameter, 7 mm thickness) were exposed to Cu K_α radiation ($\lambda = 1.5418$ Å) using a scanning speed of 2 deg min^{-1}.

A plot of intensity versus 2Θ (Θ represents Bragg angle) was obtained, illustrating peaks at different Bragg angles. The Bragg angles corresponding to different peaks were noted and the values of interplanar spacings, d, were calculated from Bragg's law. The values of d thus obtained were matched with standard values for magnesium and other phases provided in Reference [7].

2.8. Coefficient of thermal expansion

Coefficient of thermal expansion (CTE) of Mg and Mg/SiC samples was determined using an automated SETARAM 92-16/18 thermomechanical analyzer. Displacement of Mg and Mg/SiC samples (10 mm diameter, 8–11 mm length) as a function of temperature (in the range of 20–400 °C) was measured using an alumina probe under argon atmosphere and was subsequently used to determine the coefficient of thermal expansion. The heating rate of the samples was maintained at 10 °C/min while the argon gas flow rate was maintained at 1.1 lit/min.

2.9. Mechanical behavior

Mechanical behavior of extruded Mg and Mg/SiC samples was assessed in terms of their microhardness, superficial Rockwell hardness and tensile properties.

Microhardness measurements were made to provide insight into the effect of addition of SiC particulates on the microhardness of the magnesium matrix and to assess the hardness of magnesium matrix in the immediate vicinity of SiC particulates. Microhardness of Mg and Mg/SiC samples was determined using the Matsuzawa MXT50 automatic digital microhardness tester. Microhardness measurements were made using a pyramidal diamond indenter with a facing angle of 136°, 25 g indenting load, load applying speed of 50 μm/s and a load holding time of 15 s.

Macrohardness of polished unreinforced and reinforced samples was determined using the Rockwell 15T Superficial scale. Superficial Rockwell hardness measurements were made using a 1/16 inch diameter steel ball indenter with a 15 kg major load, in accordance with ASTM E18-92 standard.

The smooth bar tensile properties of the extruded Mg and Mg/SiC samples were determined in accordance with the ASTM test method E8M-96. The tensile tests were conducted on round tension test specimens of diameter 5 mm and gage length 25 mm using an automated servohydraulic INSTRON 8501 testing machine with the crosshead speed set at 0.254 mm/min.

2.10. Fracture behavior

Fracture surface characterization studies were carried out on the tensile fractured Mg and Mg/SiC samples in order to provide insight into the various fracture mechanisms operative during tensile loading of the samples. Fracture surface characterization studies were primarily accomplished using a JEOL scanning electron microscope equipped with EDS [Energy Dispersive Spectroscopy].

3. Results

3.1. Macrostructure

Macrostructural characterization conducted on the as-deposited Mg and Mg/SiC ingots revealed no evidence of blowholes and macropores and minimal presence of solidified oxide sludge. Shrinkage cavity in all the cases was very shallow and there was no evidence of any adverse reaction between the solidified melt and the graphite crucible. No evidence of gravity settling of SiC particulates could be observed in the case of Mg/SiC composites. The shrinkage cavity of Mg and Mg/SiC ingots was subsequently removed and the samples for various characterization studies and secondary processing were removed randomly from the remaining portion.

3.2. Quantitative assessment of SiC particulates

The results of chemical dissolution method conducted on Mg/SiC samples indicated successful retention of SiC particulates in the magnesium matrix. Table I shows the results in both weight and volume percentages.

3.3. Density measurements

The results of density measurements conducted on extruded Mg and Mg/SiC samples are shown in Table I. The volume percentage of the porosity computed using the experimentally determined density values and the results of the quantitative determination tests for SiC are shown in Table I.

3.4. Microstructural characterization

The results of optical and SEM studies conducted on the extruded Mg and Mg/SiC samples revealed the existence of a completely recrystallized matrix (see Fig. 2). The presence of the porosity was minimal and the distribution of SiC in the case of Mg/SiC samples was fairly uniform (see Fig. 3). The SiC particulates were located in both intergranular and intragranular locations. The size, aspect ratio and interparticulate

TABLE I Characterization results obtained from Mg and Mg/SiC samples

Material	SiC (wt. %)	SiC (vol. %)	Theoretical density (g/cm^3)	Experimental density (g/cm^3)	Porosity (vol. %)
Mg	—	—	1.7400	1.73 ± 0.0028	0.82
Mg/SiC	10.3	5.8	1.8294	1.82 ± 0.0021	0.12
Mg/SiC	16.0	9.3	1.8782	1.85 ± 0.0031	1.24
Mg/SiC	21.3	12.8	1.9293	1.92 ± 0.0053	0.68

TABLE II Microstructural characterization results obtained from Mg and Mg/SiC samples

	Characteristics of SiC particulates			Characteristics of the grains	
Material	Size (μm)	Aspect ratio	λ(μm)*	Size (μm)	Aspect ratio
Mg	—	—	—	53.3 ± 22.4	1.44 ± 0.23
Mg/10.3 SiC	21.7 ± 5.2	1.7 ± 0.3	90.1	46.4 ± 14.0	1.36 ± 0.12
Mg/16 SiC	23.7 ± 5.0	1.6 ± 0.4	77.7	40.8 ± 14.5	1.42 ± 0.13
Mg/21.3 SiC	24.6 ± 6.1	1.7 ± 0.4	68.8	34.2 ± 10.1	1.44 ± 0.15

*$\lambda = (\mathrm{l}.\ t/V_\mathrm{f})^{1/2}$ [8].

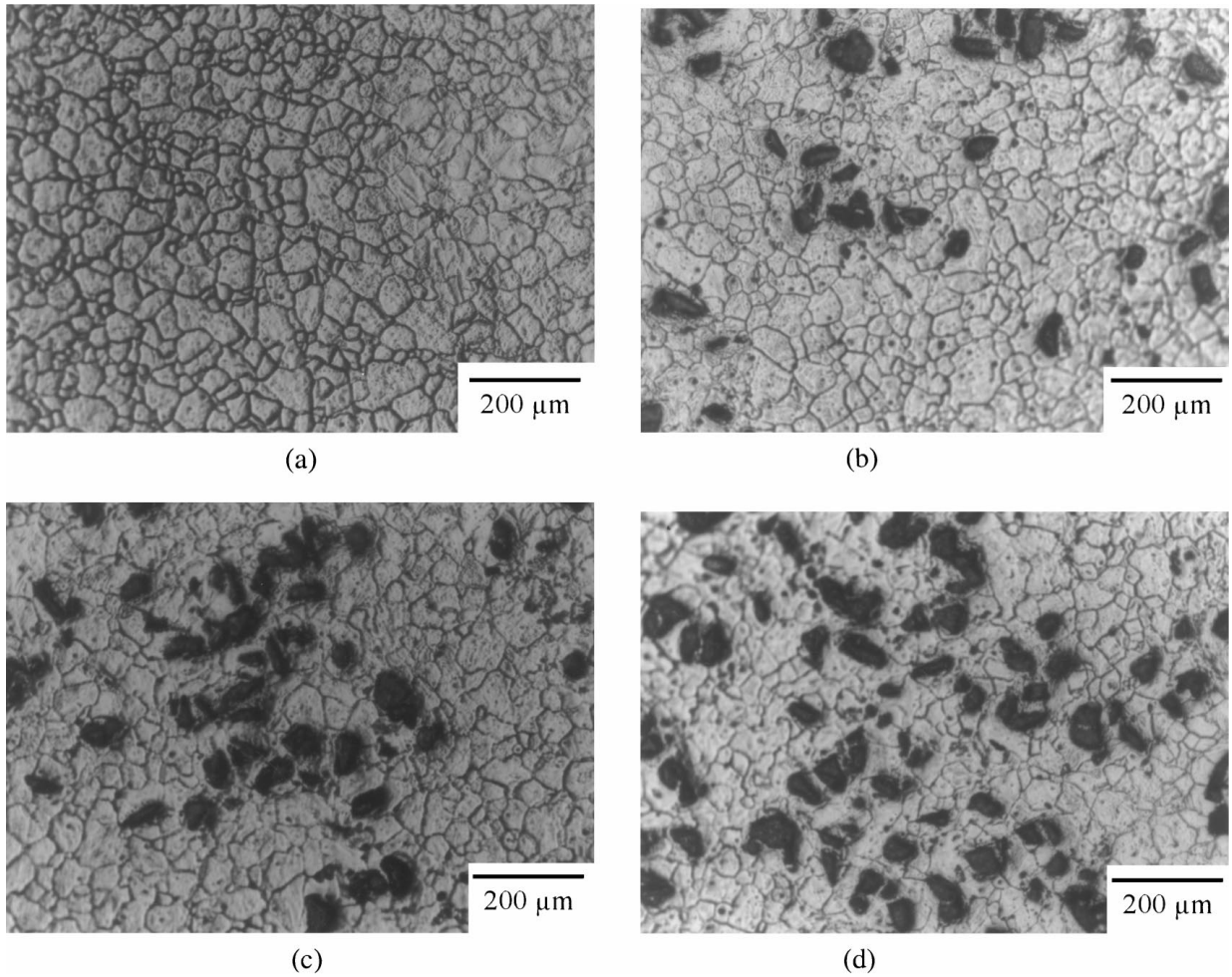

Figure 2 Representative optical micrographs showing recrystallized matrix and grain morphology in the case of: (a) Mg, (b) Mg/10.3 SiC, (c) Mg/16.0 SiC, and (d) Mg/21.3 SiC samples.

spacing (computed using the formula suggested by Nardone and Prewo [8]) of the SiC particulates in the extruded samples determined using image analysis are listed in Table II. The composite samples also exhibited to the limited extent the presence of clusters and in some cases these clusters were associated with porosity. The interfacial integrity between SiC particulates and the magnesium matrix was found to be good in all the Mg/SiC samples investigated in the present study (see Fig. 4). Unlike other composite samples investigated in the present study, the interfacial region in the case of Mg/21.3SiC samples revealed the presence of microcracks (see Fig. 4c).

3.5. X-Ray diffraction studies

The X-ray diffraction results corresponding to Mg and Mg/SiC samples were analyzed. The lattice spacings (*d*) obtained were compared with that of pure magnesium, SiC, Mg_2Si and various phases of Mg-O system. The results, in particular, show the presence of $Mg(O_2)_2$ phase in Mg/SiC samples processed using DMD route. The detailed results of the phase analysis are shown in Table III.

TABLE III Results of X-ray diffractometery studies conducted on extruded samples

		Number of matching peaks in the case of		
Phases	Mg	Mg/10.3 SiC	Mg/16 SiC	Mg/21.3 SiC
Mg	8	8	8	7
SiC(Dx:3.216)	—	4	4	3
Mg_2Si(Dx:2.096)	—	4	4	4
$Mg(O_2)_2$	4	3	3	3

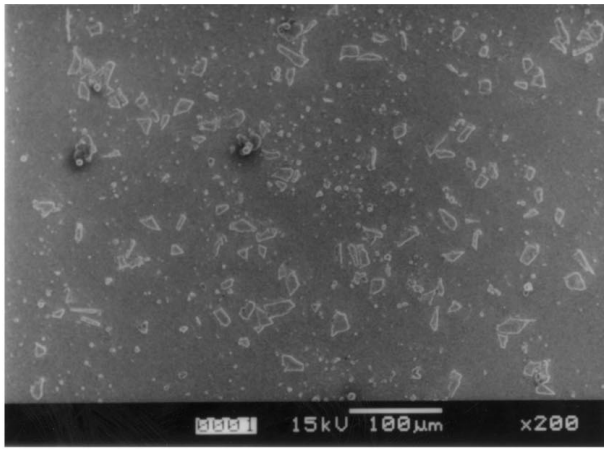

(a)

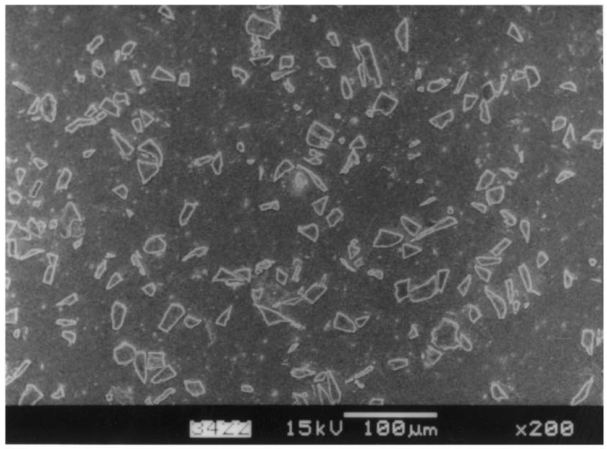

(b)

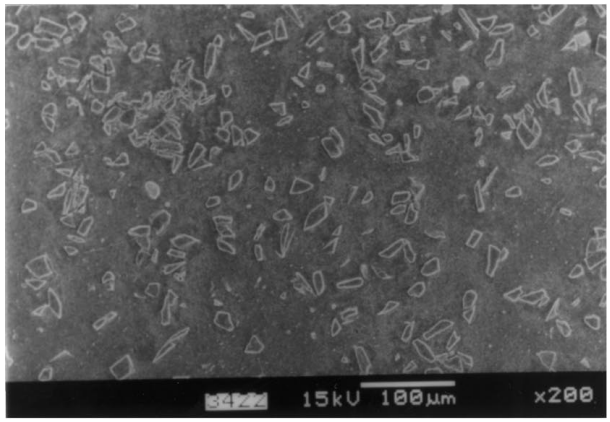

(c)

Figure 3 Representative SEM micrographs showing distribution of SiC particulates in: (a) Mg/10.3 SiC, (b) Mg/16.0 SiC, and (c) Mg/21.3 SiC samples.

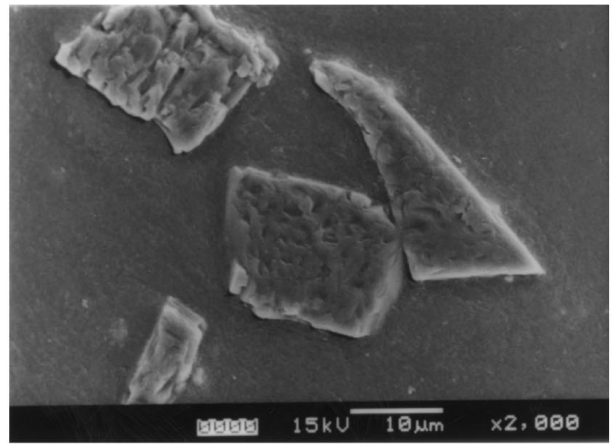

(a)

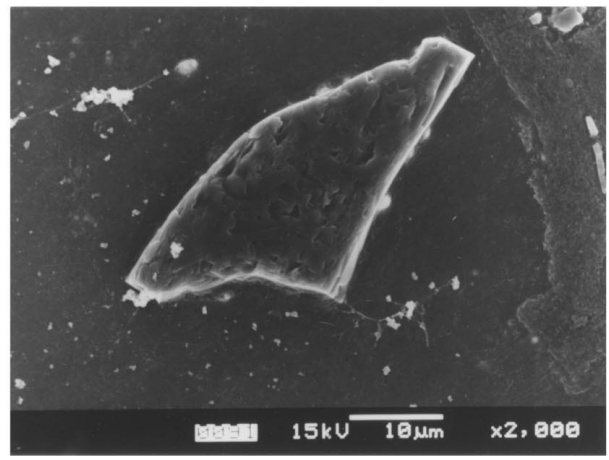

(b)

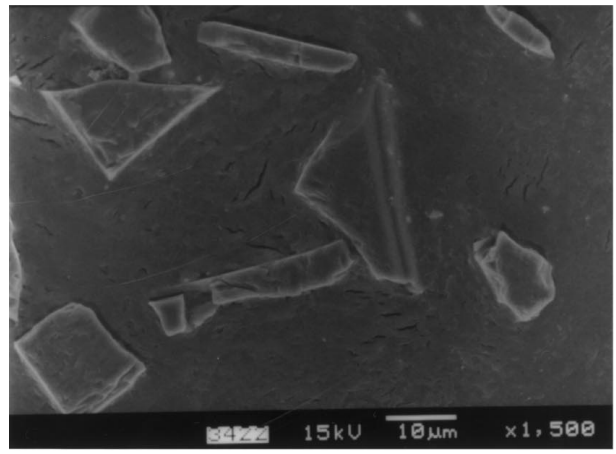

(c)

Figure 4 Representative SEM micrographs showing SiC-Mg interfacial characteristics in: (a) Mg/10.3 SiC, (b) Mg/16.0 SiC, and (c) Mg/21.3 SiC samples.

3.6. Coefficient of thermal expansion

The results of coefficient of thermal expansion (CTE) measurements obtained from Mg and Mg/SiC samples are listed in Table IV. The results show a decrease in average CTE values of the magnesium matrix with an increasing weight percentage of SiC particulates in the temperature range of 20–400 °C.

3.7. Mechanical behavior

The results of the microhardness and macrohardness measurements conducted in the matrix region showed an increasing trend with an increase in weight percentage of SiC particulates (see Table IV). The microhardness of the Mg-SiC interfacial region in the case of composite samples was found to be significantly higher when compared to that of the matrix region.

The results of the ambient temperature tensile testing on the extruded Mg and Mg/SiC samples (see Table V) reveal that an increase in the weight percentage of SiC particulates in pure magnesium increases the elastic modulus, does not affect the 0.2% yield strength

TABLE IV Results of CTE and hardness measurements

Material	CTE ($\times 10^{-6}$/°C) Experimental value	Microhardness (HV) Matrix	Microhardness (HV) SiC-Mg interface	Macrohardness (HR15T)
99.5%Mg	28.43	39.7 ± 1.6	—	75.1 ± 1.7
Mg/10.3 SiC	25.36	41.2 ± 2.9	217.9 ± 17.3	79.0 ± 1.1
Mg/16.0 SiC	23.65	42.9 ± 5.8	224.8 ± 19.8	80.1 ± 1.1
Mg/21.3 SiC	23.56	43.0 ± 1.0	261.7 ± 27.6	82.2 ± 1.1

TABLE V Results of room temperature mechanical properties

Material	E (GPa)	0.2% YS (MPa)	UTS (MPa)	Ductility (%)	Work of fracture* (J/m^3)
Mg	39.4 ± 0.6	126 ± 14.4	200 ± 5.0	11.7 ± 3.1	17.4 ± 3.5
Mg/10.3 SiC	41.2 ± 1.8	127 ± 7.2	195 ± 6.7	6.0 ± 2.3	8.9 ± 2.8
Mg/16.0 SiC	43.6 ± 2.1	120 ± 4.8	181 ± 5.9	4.7 ± 1.3	8.8 ± 2.0
Mg/21.3 SiC	50.0 ± 2.6	128 ± 1.9	176 ± 3.5	1.4 ± 0.1	3.3 ± 0.8
Mg[27] (Extruded, 13 mm)	—	69–105	165–205	5–8	—
Mg[27] (Hard rolled sheet)	—	115–140	180–220	2–10	—
Mg/10 vol.% SiC[31]	45	120	160	2	—

*Determined from engineering stress-strain diagram using EXCEL software.

(0.2% YS), and reduces the ultimate tensile strength (UTS), ductility and the work of fracture (see Table V).

3.8. Fracture behavior

The tensile fracture surfaces of Mg and Mg/SiC samples are shown in Fig. 5. The fracture surface of the Mg samples indicates a transgranular cleavage type failure mode. Fracture studies conducted on the Mg/SiC samples revealed a mixed-mode type of fracture exhibiting the evidence of matrix plastic deformation, SiC-matrix debonding and SiC particulate cracking.

4. Discussion

4.1. Synthesis of Mg and Mg/SiC materials

Synthesis of Mg and Mg/SiC materials in the present study revealed three important features:

a. minimal presence of oxide sludge indicating limited oxidation of magnesium
b. undetectable reaction between Mg and Mg/SiC melts with graphite crucible, and
c. absence of macropores and blowholes

The limited oxidation of magnesium during melting and disintegration/deposition suggests that the experimental arrangement used in this study did not permit the ingress of air/oxygen. Undetectable reaction between Mg and Mg/SiC melts with graphite crucible suggests that the temperature and time condition used during synthesis process was not sufficient to trigger the reaction between the two and, in addition, can also be attributed to the inability of magnesium to form a stable carbide [3]. Finally the absence of blowholes and macropores indicate good solidification conditions achieved and also suggests that the continuous flow of argon during the melting and deposition process did not lead to the entrapment of gases.

The results of acid dissolution conducted on Mg/SiC samples, in addition, also revealed that SiC particulates upto 21.3 weight percent can be successfully retained in the magnesium matrix. This can be attributed to the ability of magnesium to readily wet SiC particulates and is also consistent with the findings of other investigators [3, 5]. Further efforts are underway to synthesize Mg/SiC composites containing even higher amount of SiC particulates.

4.2. Microstructure

The results of microstructural characterization studies conducted on extruded Mg and Mg/SiC samples are discussed in terms of:

a. grain shape and size,
b. presence and volume percentage of porosity,
c. size and distribution of SiC particulates, and
d. SiC-Mg interfacial characteristics.

In the present study, both Mg and Mg/SiC samples in the extruded condition revealed the presence of completely recrystallized matrix characterized by near-equiaxed grains. The existence of completely recrystallized matrix suggests that the hot extrusion temperature ($>0.4T_m$, where T_m is the melting point) used in the present study was sufficient to replace the defect structure arising from extrusion process with the strain-free near-equiaxed grains (see Fig. 2). Moreover, the presence of recrystallized matrix in the case of Mg/SiC samples is also in accordance with the recrystallization criterion proposed by other investigators [9].

Relatively finer grain size exhibited by magnesium matrix as a result of presence and increasing weight percentage of SiC particulates (see Table II) can primarily be attributed to the coupled effects of: (i) capability of SiC particulates to nucleate magnesium grains during recrystallization, and (ii) restricted growth of

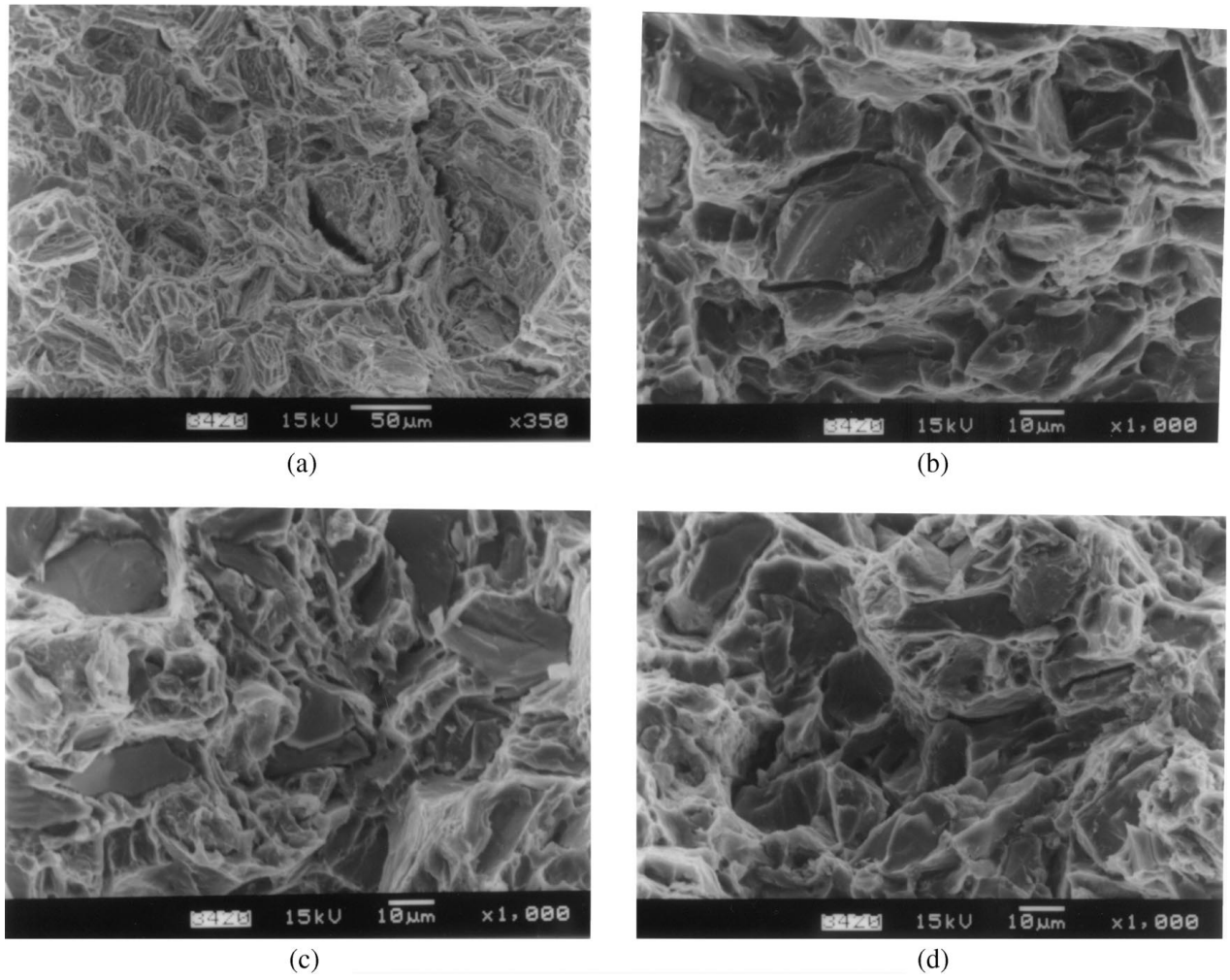

Figure 5 Representative SEM micrographs showing fracture surface characteristics of: (a) Mg, (b) Mg/10.3 SiC, (c) Mg/16.0 SiC, and (d) Mg/21.3 SiC samples.

recrystallized magnesium grains as a result of grain boundary pinning by SiC particulates. The fundamental principles behind the ability of inclusion in the metallic matrix to nucleate recrystallized grains [10] and to inhibit grain growth [11] has been already established and will not be discussed here. The results relating to the effect of SiC particulates on the grain size are also consistent with the similar effect of SiC particulates in pinning the grain boundaries in the case of aluminum based metal matrix composites when exposed at elevated temperatures [12, 13].

The results of microstructural characterization studies also revealed lower volume percent of porosity ($\leq$1.24%) retained following extrusion in the case of unreinforced and reinforced samples (see Table I). The porosity was unconnected in nature and in the case of Mg/SiC samples associated with mostly SiC particulates. Moreover, the results indicate an increase in volume percent porosity with the presence of SiC particulates. These results are consistent with the findings of Laurent *et al*. obtained on compocast AZ91D alloy reinforced with SiC particulates [5] and are also similar to the results obtained in the case of aluminum based composites [12].

Regarding SiC particulates, the results of quantitative metallographic analysis revealed that the processing methodology used in the present study led to minimal breakage of SiC particulates (see Table II). The breakage of SiC particulates during primary processing and extrusion can not be avoided as a result of mechanical stirring effect associated with former [1] and extensive axial and shear stresses associated with the later process [14]. The breakage of SiC particulates during extrusion, in addition, can also be attributed to higher tendency of SiC particulates to break under load when their size exceeds 12 μm [15].

The distribution of SiC particulates was mostly uniform and can be attributed to: (i) ability of magnesium to wet SiC particulates [3, 5], (ii) disintegration of composite slurry prior to solidification by inert gas jets [6], and (iii) redistribution of SiC particulates during extrusion as a result of different deformation modes in operation across the cross-section of the extruding billet [14, 16]. The presence of SiC particulates predominantly at grain boundaries in Mg/SiC samples can be attributed to the sequential events involving particulate pushing by solid-liquid interface as a result of sluggish solidification front velocity during solidification [3] followed by nucleation of recrystallized grains during hot extrusion at the previous grain boundaries [10]. The first stage of these events thus lead to the segregation of SiC particulates predominantly at the grain boundaries while the second stage essentially retains the original location pattern of SiC particulates. The grain boundary

location of SiC particulates, in addition, is also aided by the solid state nucleation capability of SiC particulates [10]. The results of this study, in essence, thus indicate that hot extrusion in the case of Mg/SiC composites may not be useful in changing the grain boundary location of the SiC particulates to intragranular location.

Mg-SiC interfacial integrity assessed in terms of interfacial debonding and presence of voids, was found to be very good and, in addition, did not reveal the presence of any interfacial reaction products when examined under scanning electron microscope (see Fig. 4). The results indicate the suitability of superheat temperature (750 °C) used in this study to synthesize Mg/SiC composite. In related studies [3] similarly clean and featureless surface of SiC particulates was reported for a superheat temperature of 700 °C. The results of x-ray diffraction studies conducted on Mg/SiC samples (see Table III), however, revealed the presence of Mg_2Si and $Mg(O_2)_2$ phases besides Mg and SiC phases. The results indicate that the temperature and time conditions selected during processing were sufficient for minimal reaction between molten magnesium and SiC particulates. Considering that SiC particulates contains free silicon and are often associated with a thin layer of SiO_2 [17], the possible reactions can be written as [18]:

$$2Mg + Si = Mg_2Si \quad (1)$$

$$4Mg + SiO_2 = Mg_2Si + 2MgO \quad (2)$$

The presence of Mg_2Si thus detected in this study is in accordance with the theoretical speculation and experimental findings of other investigators [18]. The reaction leading to the formation of $Mg(O_2)_2$, however, is still not clear and further work is continuing in this area.

4.3. Coefficient of thermal expansion

The results of CTE measurements in the temperature range of 20–400 °C revealed that the presence and increasing weight percentage of SiC particulates reduces progressively the average CTE value of the magnesium matrix. For comparison purpose, CTE values for the three composite samples were computed using the Rule of Mixture (upper bound, Equation 3a), Turner's model (lower bound, Equation 3b), and Kerner's model (Equation 3c) [19], respectively:

$$\alpha_{comp} = \alpha_m V_m + \alpha_r V_r \quad (3a)$$

$$\alpha_{comp} = (\alpha_m V_m K_m + \alpha_r V_r K_r)/(V_m K_m + V_r K_r) \quad (3b)$$

$$\alpha_{comp} = \alpha_m - V_r(\alpha_m - \alpha_r) \times \frac{K_m(3K_r + 4G_m)^2 + (K_r - K_m)\left(16G_m^2 + 12G_m K_r\right)}{(4G_m + 3K_r)[4V_r G_m(K_r - K_m) + 3K_r K_m + 4G_m K_m]} \quad (3c)$$

where α, V, K and G represent coefficient of thermal expansion, volume fraction, bulk modulus and shear modulus of the phase while the subscripts m and r refer to the matrix and reinforcement, respectively. Using the values of $\alpha_m = 28.43 \times 10^{-6}/°C$, $K_m = 35.6$ GPa, $G_m = 17$ GPa, $\alpha_r = 4.63 \times 10^{-6}/°C$, and $K_r = 221$ GPa (see Table I and References [20, 21]), the coefficient of thermal expansion of the composites were computed and shown in Fig. 6 with the experimentally obtained values. Fig. 6 reveals that the experimental values follow the similar trend as the theoretically computed values and are close to predictions made by the Kerner model. In related studies, investigators reported that the CTE values of ZK60A magnesium alloy reinforced with particulate SiC and particulate B_4C reinforcements follow closely the Kerner's prediction [19]. Relatively lower magnitude exhibited by the experimental values when compared to the Kerner's predictions indicates optimal realization of physical properties of the reinforcement and can be attributed to the coupled influence of: a) uniform distribution of SiC particulates, and b) good interfacial integrity between SiC particulates and the magnesium matrix. The results obtained in this study thus indicate that a high dimensional stability can be achieved in the case of Mg/SiC composites synthesized using disintegrated melt deposition technique.

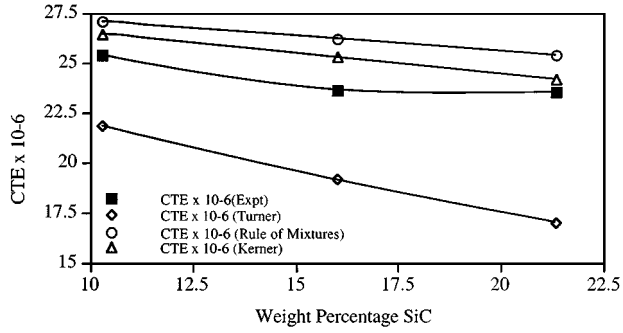

Figure 6 Graphical representation showing the theoretically computed and experimentally obtained CTE values as a function of weight percentage of SiC particulates.

4.4. Mechanical behavior

The results of hardness measurements revealed that an increase in the weight percentage of SiC particulates lead to: a) an increase in the microhardness of the metallic matrix, b) an increase in the hardness of the SiC-Mg interfacial region, and c) an increase in the overall (bulk) hardness of the composite material (see Table IV). This can be attributed to the: i) increasing presence of harder SiC particulates [12] in the matrix, ii) higher constraint to the localized matrix deformation during indentation as a result of increasing presence of SiC particulates, and iii) increasing ability of SiC particulates to refine matrix microstructure (see Table II). These results are consistent with the similar findings obtained on aluminum based composite materials [22]. Significantly higher SiC-Mg interfacial hardness values when compared to the matrix microhardness values (see Table IV) observed in the case of composite samples can be attributed to: i) higher density of dislocations in the immediate vicinity of SiC particulates as a result of significant difference in coefficient of thermal expansion between magnesium and SiC particulates (6.24 : 1) [1, 20, 21], and ii) presence of intermetallics originating from interfacial reaction between SiC particulates and

magnesium matrix (see Table III). Further work using transmission electron microscopy is continuing in this area.

The results of elastic modulus measurements revealed that an increase in the weight percentage of SiC particulates lead to an increase in the elastic modulus of the magnesium matrix. This can primarily be attributed to the higher elastic modulus of SiC particulates when compared to that of magnesium [23]. In order to compare the experimental results with the theoretical predictions, Elastic modulus values were also computed using Halpin-Tsai equation [1]. Halpin-Tsai equation can be expressed as:

$$E_c = \frac{E_m(1 + 2sqV_r)}{1 - qV_r} \tag{4}$$

where, E_c and E_m represent the Elastic modulus of composite and metallic matrix, respectively, while V_r represent the volume fraction of the reinforcement. The term, q, in Equation 4 can be represented as:

$$q = \frac{E_r/E_m - 1}{E_r/E_m + 2s} \tag{5}$$

where, E_r represent the elastic modulus of the reinforcement and s represent the aspect ratio of the reinforcing phase. The values of $E_r = 450$ GPa [23], $E_m = 39.4$ GPa (see Table V) and s from Table II were used in Equations 4 and 5 in order to compute the Elastic modulus values for the composites investigated in the present study. The theoretically computed values along with the experimental values are shown in Fig. 7. The results show that while the experimentally determined values follow the same trend as of theoretically computed values, their magnitude remained lower. One of the reason for such behavior is the presence of finite amount of non-connected porosity following extrusion in the composite samples (see Table I). The presence of such porosity may adversely affect the elastic response of the materials as a result of reduction in effective load bearing area [24]. A model was proposed recently [25] that correlates the elastic modulus of the porous material (E) with the elastic modulus of the fully dense material (E_o) and the volume fraction of the pores (p) through the following equation [24, 25]:

$$E = E_o(1 - p^{2/3})^{1.21s} \tag{6}$$

where the power factor s in Equation 6 is

$$s = (z/x)^{1/3}\left\{1 + [(z/x)^{-2} - 1]\cos^2\alpha_d\right\}^{1/2} \tag{7}$$

where z/x is the aspect ratio of the pores and α_d represents the relative orientation of the pores with respect to stress axis. The orientation factor $\cos^2\alpha_d$ is equivalent to 0.31 for material with a random orientation of pores which correspond to an α_d of 56° [24]. Assuming $z/x = 1$, the elastic modulus were computed for the three composite materials and are shown in Fig. 7. The computation results clearly exhibited an upward correction indicating the achievable elastic modulus from the three composite materials synthesized in the present study. The porosity corrected elastic modulus values, however, still remained lower than the values predicted by Halpin Tsai equation and this can be attributed to the comparatively non-uniform distribution of SiC particulates and less than ideal SiC-Mg interfacial integrity. It may be noted that any deviation from the uniform distribution and perfectly bonded interface will result into the significant lowering of internal stress between SiC particulates and the matrix which is essential for realizing an increase in elastic modulus [3]. The results obtained in the present study are also consistent with the trend exhibited by cast Al-SiC composites [26].

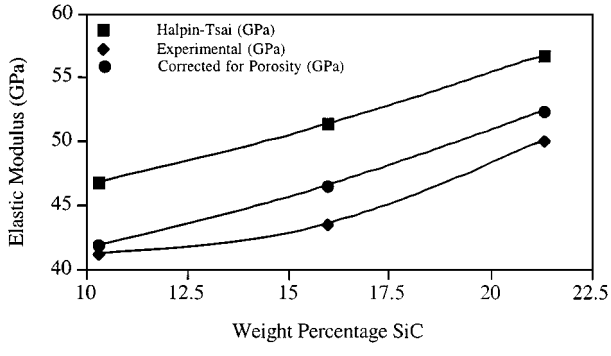

Figure 7 Graphical representation showing the theoretically computed and experimentally obtained elastic modulus values as a function of weight percentage of SiC particulates.

The results of tensile properties characterization revealed that increasing presence of SiC particulates in the magnesium matrix did not affect 0.2% YS and reduced UTS, ductility and work for fracture (see Table V). The similar values of 0.2% YS obtained in the case of unreinforced and reinforced samples indicated that the presence of SiC particulates within the limits of 21.3 weight percent and reduction in grain size as a result of presence of SiC particulates were not sufficient to realize the substantial increase in the resistance of material towards deformation upto a strain level of 0.002. It may very interestingly be noted that the 0.2% YS achieved in the case of Mg samples was superior when compared to the values reported in Reference [27] for extruded samples and this may primarily be attributed to the experimental parameters chosen for the secondary processing. A similar dependence of the tensile properties of magnesium on the secondary processing is reproduced in Table V [27].

The lower value of UTS, ductility and work of fracture exhibited by Mg/SiC samples when compared to Mg samples and the reduction in these properties with an increasing presence of SiC particulates can primarily be attributed to the reduced cavitation resistance of magnesium matrix due to the combined presence of porosity and SiC particulates [28–30]. In related studies conducted on as-cast AZ91/SiC composites [3], for example, investigators proposed that the presence of SiC particulates lead to localized damages such as particulate cracking and interface debonding resulting into lower elongation values. In yet another study conducted on extruded rheocast AZ91D based materials,

investigators reported similar trend of reduction in elongation and UTS values as a result of presence of SiC particulates [5].

It may however be noted that the overall combinations of strength and ductility values realized in the case of DMD processed Mg/SiC composites are much superior (see Table V) when compared to the values reported by other investigators for the composites based on Mg/SiC formulation and synthesized using molten metal based methods [31].

4.5. Fracture behavior

The results of fracture surface analysis revealed a typical brittle fracture in the case of Mg samples (see Fig. 5). This can be attributed to the HCP crystal structure of magnesium that restricts the slip to the basal plane. The presence of small steps and microscopically rough fracture surface indicates the inability of magnesium to cleave on any single plane consistent with the findings reported elsewhere [11].

In the case of Mg/SiC samples, evidence of areas of extensive plastic deformation adjacent to SiC particulates is indicative of strain accumulation at the SiC-Mg interface (see Fig. 5) and the presence of broken SiC particulates with minimal interfacial debonding indicates a good interfacial bond realized between SiC particulates and magnesium matrix using the present experimental methodology. The presence of broken SiC particulates, however, may also be attributed to: (i) their size (>12 μm) that may promote easy fracture during tensile loading [15], (ii) as a result of thermal shock during solidification [18], and (iii) during extrusion process. Further work is continuing in order to determine and delineate the predominant mechanism that leads to the presence of broken SiC particulates on the tensile fractured samples.

In essence, the results of fractographic analyses obtained in the present study are consistent with the findings reported elsewhere [3, 18] for Mg-based materials and the SiC associated localized damages are qualitatively similar to those exhibited by aluminum-based materials [1, 12, 17, 30].

5. Conclusions

The primary conclusions that may be derived from this work are as follows:

1. Disintegrated melt deposition and hot extrusion methodology used in the present study can be successfully utilized to synthesize elemental and silicon carbide reinforced magnesium with minimal porosity.

2. Good distribution of SiC particulates and SiC-Mg interfacial integrity achieved in the present study indicate the suitability of the selection of experimental parameters during primary processing (such as superheat temperature and stirring methodology) and secondary processing (such as extrusion ratio).

3. The results of coefficient of thermal expansion measurements indicate that the increasing presence of SiC particulates lead to progressive reduction in CTE value of the magnesium matrix.

4. The improved combination of tensile strengths and ductility in the case of elemental magnesium when compared to the published values for extruded samples can primarily be attributed to the processing (primary + secondary) methodology adopted in the present study. The results also showed that the increasing presence of SiC particulates improves hardness and elastic modulus, does not affect 0.2% yield strength, and lowers ultimate tensile strength, ductility and work of fracture.

5. The results of fracture surface characterization revealed that SiC particulate cracking is the predominant localized damage mechanism under tensile loading in the case of reinforced magnesium samples.

Acknowledgments

The authors would like to thank NUS (grant # RP 3970653) for financial support during the course of this investigation. In addition, the authors would also like to thank Mr. Thomas Tan, Mr. Boon Heng and Mr. N. Srikanth for their valuable assistance and for many useful discussions and to Ms Neerja Gupta for improving the readability of this manuscript.

References

1. D. J. LLOYD, *Int. Mat. Reviews* **39**(1) (1994) 1.
2. D. M. LEE, B. K. SUH, B. G. KIM, J. S. LEE and C. H. LEE, *Mat. Sci. Tech.* **13** (1997) 590.
3. A. LUO, *Metall. Mater. Trans.* **A26** (1995) 2445.
4. J. LO and G. CARPENTER, in "Conf. Proceedings of ICCE/5," edited by D. Hui (Las Vegas, July 5–11, 1998) p. 526.
5. V. LAURENT, P. JARRY, G. REGAZZONI and D. APELIAN, *J. Mat. Sci.* **27** (1992) 4447.
6. M. GUPTA, M. O. LAI and C. Y. SOO, *Mat. Sci. and Eng.* **A210** (1996) 114.
7. Powder Diffraction File, International Center for Diffraction Data, 1601 Park Lane, Swarthmore, PA, USA, 1991.
8. V. C. NARDONE and K. W. PREWO, *Scr. Metall.* **20** (1986) 43.
9. W. S. MILLER and F. J. HUMPHREYS, *Scr. Metall. et Mater.* **25** (1991) 2623.
10. P. G. SHEWMON, "Transformation in Metals" (McGraw-Hill Book Company, New York, USA, 1969) p. 69.
11. R. E. REED-HILL, "Physical Metallurgy Principles," 2nd ed. (D. Van Nostrand Company, New York, USA, 1964) pp. 267, 753.
12. M. GUPTA, F. MOHAMED, E. LAVERNIA and T. S. SRIVATSAN, *J. Mat. Sci.* **28** (1993) 2245.
13. M. GUPTA, F. A. MOHAMED and E. J. LAVERNIA, *Metall. Trans.* **23A** (1992) 845.
14. M. GUPTA, R. SIKAND and A. K. GUPTA, *Scr Met et Mater.* **30**(10) (1994) 1343.
15. Z. G. WANG, S. LI and L. SUN, *Key Eng. Mater.* **104–107** (1995) 729.
16. M. K. SURAPPA, *J. Mat. Sci. Lett.* **12** (1993) 1272.
17. M. GUPTA, I. A. IBRAHIM, F. MOHAMED and E. LAVERNIA, *J. Mat. Sci.* **26** (1991) 6673.
18. B. INEM and G. POLLARD, *ibid.* **28** (1993) 4427.
19. A. L. GEIGER and M. JACKSON, *Adv. Mat. Proc.* **136**(7) (1989) 23.
20. C. J. SMITHELLS, "Metals Reference Book," 5th ed. (Butterworths & Co. Ltd, London, 1976).
21. J. F. SHACKELFORD, W. ALEXANDER and J. S. PARK, "CRC Materials Science and Engineering Handbook" (CRC Press Inc., 1994) p. 304.
22. M. GUPTA and S. LING, *Mater. and Design* **18**(3) (1997) 139.
23. N. CHRISTMAN and S. SURESH, *Acta. Metall.* **36** (1988) 1691.
24. G. E. FOUGERE, L. RIESTER, M. FERBER, J. R. WEERTMAN and R. W. SIEGEL, *Mater. Sci. and Eng. A*, **204** (1995) 1.

25. A. R. BOCCACCINI, G. ONDRACEK, P. MAZILU and D. WINDELBERG, *J. Mech. Behav. Mater*. **4** (1993) 119.
26. M. GUPTA and M. K. SURAPPA, *Key Eng. Mater*. **104**–**107**, Part 1 (1995) 259.
27. ASM Handbook, "Properties and Selection: Nonferrous Alloys and Special-purpose Materials, Vol. 2" (ASM International, 1990) p. 1132.
28. G. F. BOCCHINI, *Int. J. of Powder Metallurgy* **22**(3) (1986) 185.
29. R. D. PAYNE, A. L. MORAN and R. C. CAMMARATA, *Scr. Metall. et Mater*. **29** (1993) 907.
30. D. L. MCDANELS, *Metall. Trans*. **A16** (1985) 1105.
31. M. R. KRISHNADEV, R. ANGERS, C. G. KRISHNADAS NAIR and G. HUARD, *J. Met*. **45**(8) (1993) 52.

Received 24 June
and accepted 1 November 1999